AGU PUBLICATIONS

JGR

Journal of Geophysical Research: Oceans

RESEARCH ARTICLE

10.1002/2016JC012115

Distribution of water masses and meltwater on the continental shelf near the Totten and Moscow University ice shelves

Alessandro Silvano[1,2], Stephen R. Rintoul[2,3], Beatriz Peña-Molino[3], and Guy D. Williams[1,3,4]

[1]Institute for Marine and Antarctic Studies, University of Tasmania, Hobart, TAS, Australia, [2]CSIRO Oceans & Atmosphere, Hobart, TAS, Australia, [3]Antarctic Climate and Ecosystems Cooperative Research Centre, University of Tasmania, Hobart, TAS, Australia, [4]Antarctic Research Council Centre of Excellence for Climate System Science, University of New South Wales, Sydney, NSW, Australia

Key Points:
- Warm (up to 0.3°C) modified Circumpolar Deep Water is widespread on the continental shelf, overlaid by fresh Winter Water
- A series of deep troughs allows relatively warm water to reach the ice-shelf cavities and drive basal melt
- Freshening by addition of glacial meltwater is extensive on the inner shelf at depths above 300–400 m

Correspondence to:
A. Silvano,
Alessandro.Silvano@utas.edu.au

Citation:
Silvano, A., S. R. Rintoul, B. Peña-Molino, and G. D. Williams (2017), Distribution of water masses and meltwater on the continental shelf near the Totten and Moscow University ice shelves, *J. Geophys. Res. Oceans*, *122*, 2050–2068, doi:10.1002/2016JC012115.

Received 1 JUL 2016
Accepted 7 FEB 2017
Accepted article online 11 FEB 2017
Published online 16 MAR 2017

Abstract Warm waters flood the continental shelf of the Amundsen and Bellingshausen seas in West Antarctica, driving rapid basal melt of ice shelves. In contrast, waters on the continental shelf in East Antarctica are cooler and ice shelves experience relatively low rates of basal melt. An exception is provided by the Totten and Moscow University ice shelves on the Sabrina Coast, where satellite-derived basal melt rates are comparable to West Antarctica. Recent oceanographic observations have revealed that relatively warm (~−0.4°C) modified Circumpolar Deep Water (mCDW) enters the cavity beneath the Totten Ice Shelf through a 1100 m deep trough, delivering sufficient heat to drive rapid basal melt. Here we use observations from a recent summer survey to show that mCDW is widespread on the continental shelf of the Sabrina Coast, forming a warm (up to 0.3°C) and saline (34.5–34.6) bottom layer overlaid by cold (~freezing point) and fresh (salinity ~34.3) Winter Water. Dense Shelf Water is not observed. A 1000 deep m trough allows water at −1.3°C to reach the Moscow University ice-shelf cavity to drive basal melt. Freshening by addition of glacial meltwater is widespread on the southern shelf at depths above 300–400 m, with maximum meltwater concentrations up to 4–5 ml L^{-1} observed in outflows from the ice-shelf cavities. Our observations indicate that the ocean properties on the Sabrina Coast more resemble those found on the continental shelf of the Amundsen and Bellingshausen seas than those typical of East Antarctica.

Plain Language Summary The Totten Glacier drains more ice from the East Antarctic Ice Sheet than any other glacier. The Totten holds a volume of ice equivalent to more than 3.5m of global sea level rise, so changes in the glacier could have significant consequences. East Antarctic ice shelves, including the Totten, were thought to be largely isolated from warm ocean waters and therefore stable. An Australian voyage in 2015 obtained the first oceanographic data near the Totten and Moscow University Ice Shelves. The measurements show that relatively warm water spreads from the open ocean across the continental shelf to reach the ice shelf cavities, where it drives melt of the underside of the ice shelves. The presence of warm water near the ice shelves helps explain rapid rates of melt inferred from satellite data. The study shows that this part of the East Antarctic Ice Sheet is more exposed to warm ocean waters, and therefore may make a larger contribution to sea level rise, than previously thought.

1. Introduction

The Antarctic Ice Sheet flows toward the coast through several outlet glaciers. Floating ice shelves form where an outlet glacier reaches the ocean. Back stresses generated by interaction of the flowing ice shelves with side-walls and topographic rises can restrain ("buttress") the glacial flow into the ocean [*Dupont and Alley*, 2005]. A thinning or collapse of the buttressing ice shelves would reduce the restraint on the glacial flow, increasing the ice discharge into the ocean. Acceleration during the last few decades in the flow of some of the outlet glaciers has led to a dramatic increase in Antarctic ice loss, with most of the ice discharge occurring along the coast of the Amundsen and Bellingshausen seas in West Antarctica [*Rignot et al.*, 2008; *Harig and Simons*, 2015; *Wouters et al.*, 2015]. Here the ice loss has been primarily attributed to thinning of the buttressing ice shelves as a result of rapid basal melt by ocean heat flux [*Shepherd et al.*, 2004; *Pritchard et al.*, 2012].

The ocean heat flux in West Antarctica is associated with intrusions of warm (>0°C), salty (>34.5), and slightly modified Circumpolar Deep Water (mCDW) onto the continental shelf. This warm water fills the bottom

layer and is able to access the cavity beneath several ice shelves to drive rapid basal melt [*Jenkins and Jacobs*, 2008; *Jacobs et al*., 2011; *Dutrieux et al*., 2014; *Jacobs et al*., 2013]. Winter convection does not extend to sufficient depth to destratify the water column and erode the mCDW in these regions, resulting in a shallow mixed layer overlying the warm mCDW [*Petty et al*., 2013].

In many other parts of Antarctica, active coastal polynyas drive strong convection in winter. Polynyas are regions of enhanced sea-ice formation, where water masses are transformed by local processes such as atmospheric cooling, wind stress, and brine rejection. In the strongest polynyas, the wintertime convection from sea-ice formation is sufficient to overturn the entire water column to produce cold ($\sim$surface freezing point) and saline ($>$34.5) Dense Shelf Water (DSW). Examples of strong polynyas are found in the Ross Sea [*Jacobs et al*., 1970], in the Weddell Sea [*Gill*, 1973], and in several areas in East Antarctica, such as the Adélie Coast [*Rintoul*, 1998], Vincennes Bay [*Kitade et al*., 2014], and Prydz Bay/Cape Darnley [*Williams et al*., 2016; *Ohshima et al*., 2013]. DSW formed in these regions overflows the shelf break and cascades down the slope, mixing with ambient water to form Antarctic Bottom Water, thus contributing to the global overturning circulation [*Johnson*, 2008; *Marshall and Speer*, 2012].

Part of the DSW produced in these polynyas is able to access the cavities of nearby ice shelves. Since the sea floor usually gets deeper toward the grounding line of an ice shelf, DSW spreads along the sea floor to reach the deepest areas near the grounding line [*Jacobs et al*., 1992]. The depression of the seawater freezing point with increasing pressure, $\sim$0.75°C every 1000 dbar [*Foldvik and Kvinge*, 1974], means that the DSW is warmer than the local freezing point and therefore able to melt the base of the ice shelf.

East Antarctic ice shelves located in regions where cold DSW is formed (e.g., the Mertz Glacier Tongue on the Adélie Coast and the Amery Ice Shelf in Prydz Bay) experience low area-averaged rates of basal melt (typically less than 2 m yr^{-1}) compared to the Amundsen and Bellingshausen seas where rates are usually higher than 4–5 m yr^{-1}, reaching values up to 15–20 m yr^{-1} at the floating ends of Pine Island and Thwaites glaciers [*Rignot et al*., 2013; *Depoorter et al*., 2013; *Liu et al*., 2015]. However, an exception is provided by ice shelves located on the Sabrina Coast, namely the Totten and Moscow University ice shelves (TIS and MUIS, respectively, Figure 1), which show rates of basal melt ($>$4 m yr^{-1}) comparable with those observed in the Amundsen and Bellingshausen seas.

TIS and MUIS represent the floating ends of the Totten and Moscow University glaciers, respectively. These glaciers drain a large sector of the marine-based Aurora Subglacial Basin and understanding their stability is important for determining the future contribution of this sector of the East Antarctic Ice Sheet to global sea level [*Sun et al*., 2016]. The Totten Glacier alone drains a volume of ice above flotation equivalent to 3.5 m of sea-level rise, an amount similar to the entire West Antarctic Ice Sheet [*Greenbaum et al*., 2015]. Two recent studies show that the grounded part of the Totten Glacier has experienced sustained thinning (0.7 ± 0.1 m yr^{-1}) and mass loss (7 ± 2 Gt yr^{-1}) during the past two decades [*Li et al*., 2015, 2016]. Satellite estimates suggest that the TIS has experienced periods of thinning and thickening, with no significant trend during the past 20 years [*Paolo et al*., 2015]. Ocean modeling studies suggest that mCDW is able to access the TIS cavity to drive basal melt [*Khazendar et al*., 2013; *Gwyther et al*., 2014]. The model results indicate that ocean heat flux to the cavity is regulated by the activity of the Dalton Polynya (DP) east of the TIS (Figure 1). When sea-ice production is higher than average, cold water formed in the polynya mixes with the mCDW that intrudes onto the continental shelf, reducing the temperature of water reaching the ice-shelf cavity. When sea-ice production is lower, mCDW reaches the TIS cavity in a less modified form and drives more basal melt, possibly triggering a thinning of the Totten Glacier.

Measurements collected on the outer continental shelf of the Sabrina Coast show the presence of warm mCDW near the sea floor in summer 1996 and late winter 2007, and no evidence of DSW [*Bindoff et al*., 2000; *Williams et al*., 2011]. More recently, *Rintoul et al*. [2016] used observations from the TIS calving front to quantify exchange with the ice-shelf cavity. They found that warm mCDW entered the TIS cavity through a deep trough at the calving front, the Totten Trough, and carried sufficient heat to sustain an area-averaged basal melt rate $>$10 m yr^{-1}, in agreement with satellite observations [*Rignot et al*., 2013; *Depoorter et al*., 2013; *Liu et al*., 2015]. The TIS basal melt rate is the highest observed on the Sabrina Coast and the largest among the East Antarctic ice shelves with an area bigger than 1000 km^2 [*Silvano et al*., 2016]. Here we use an extended data set to show the spatial variability of the ocean properties on the continental shelf of the Sabrina Coast and to describe how ocean heat is transported to the MUIS and TIS. Our results from

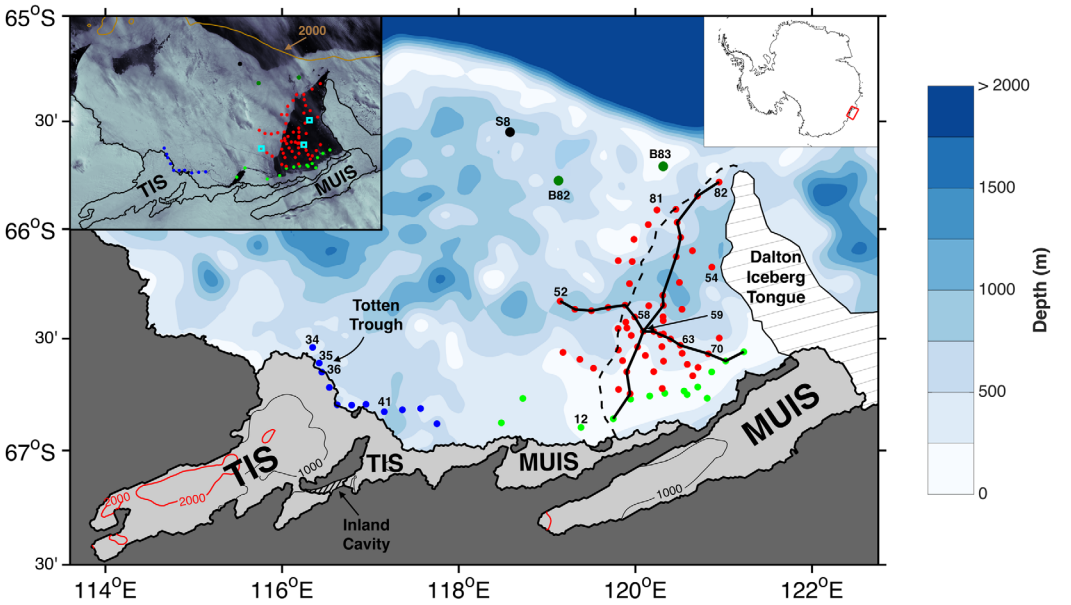

Figure 1. Map of the survey area. Overlaid is the bathymetry and the coastline [Bedmap2, *Fretwell et al.*, 2013]. Bathymetry from geophysical data beneath the Totten Ice Shelf (TIS) is included [*Greenbaum et al.*, 2015]. Red, green, and blue dots indicate the stations collected in the Dalton Polynya (DP), in proximity to the Moscow University Ice Shelf (MUIS) and TIS calving fronts, respectively. The location of stations 82 and 83 from BROKE is shown in dark green (B82–B83), while station 8 from SIPEX is shown in black (S8). The inland cavity identified by *Greenbaum et al.* [2015] and the Totten Trough (located near stations 35 and 36) are highlighted. The dashed white area north of the MUIS is the Dalton Iceberg Tongue, a combination of grounded icebergs and fast ice. The black lines highlight the two transects shown in Figures 2 and 3. The dashed line indicates the approximate eastern boundary of the area covered by sea ice. Stations shown in Figures 5, 6, 8, 10, and 11 are labeled. In the inset on the upper-left corner is a MODIS [*Scambos et al.*, 1996] image (22 January 2015) with coastline overlaid. Light blue squares are the location of the moorings, while the brown line is the 2000 m isobath which shows the approximate location of the continental slope.

the Sabrina Coast are then compared with two other sites around Antarctica, Pine Island Bay in West Antarctica, and the Adélie Coast in East Antarctica.

2. Data

A survey was conducted on the shelf of the Sabrina Coast (115°E–125°E) on the R/V *Aurora Australis* (cruise AU1402) between 23 December 2014 and 6 January 2015 (Figure 1). We show the results from the analysis of 81 CTD stations collected during this expedition (Figure 1). CTD data include continuous profiles of temperature (°C), salinity (PSS78), pressure (dbar), and dissolved oxygen (μmol L^{-1}). Data were vertically averaged in 2 dbar bins with calibration performed using bottle samples [*Rosenberg and Rintoul*, 2016]. Uncertainties on the measurements of temperature, salinity, and pressure are ~0.001°C, 0.002 (PSS78), and 1 dbar, respectively. The relative uncertainty on the dissolved oxygen data is ~1%. Three moorings were deployed on the continental shelf between 300 m and the bottom (see the inset in Figure 1 for location) in February 2014 during the NBP1402 expedition on the US R/V *Nathaniel B. Palmer* and recovered in January 2015 during the AU1402 voyage. At each mooring, temperature and salinity data were collected at four equally spaced depths [*Rosenberg and Rintoul*, 2016]. Individual time series shows decorrelation time scales exceeding 2 weeks (i.e., the duration of our survey on the Sabrina Coast), with an average value of about 30 days, confirming the synopticity of the survey.

We compare our measurements to data collected on two previous surveys on the continental shelf of the Sabrina Coast. Two CTD stations were occupied in austral summer 1996 during Baseline Research on Oceanography Krill and the Environment (BROKE) [*Bindoff et al.*, 2000] (Figure 1). Temperature from a single ice station in late winter 2007 during Sea Ice Physics and Ecosystem eXperiment (SIPEX) is also used [*Williams et al.*, 2011] (Figure 1). We also compare our data to measurements of temperature, salinity, and dissolved oxygen from the Adélie Coast in East Antarctica and from Pine Island Bay in West Antarctica. Data from the Adélie Coast were collected during the AU1402 voyage after the survey of the Sabrina Coast, while measurements from Pine Island Bay were collected in austral summer 2009 [*Jacobs et al.*, 2011].

3. Results

3.1. Water Mass Classification

A meridional section in the DP reveals four water masses present on the shelf (Figure 2). Relatively warm and salty mCDW is found near the sea floor. Neutral density is not well defined in regions where few data are available, as on the continental shelf of the Sabrina Coast; therefore, we use surfaces of potential density anomaly referenced to the surface, σ_θ, to define different layers. The $\sigma_\theta = 27.7$ kg m^{-3} isopycnal is chosen to define the upper boundary of mCDW. The mCDW is the densest water mass found on the shelf during the survey; no DSW was observed.

A homogeneous layer of remnant Winter Water (WW), a product of wintertime convection, lies above the mCDW. The WW temperature is close to the surface freezing point (~−1.8°C). A thin layer of warm Antarctic Surface Water (AASW) produced by summer heating overlies the WW. The $\sigma_\theta = 27.55$ kg m^{-3} surface appears to be a reasonable boundary between WW and AASW (Figure 2a). However, in order to capture the

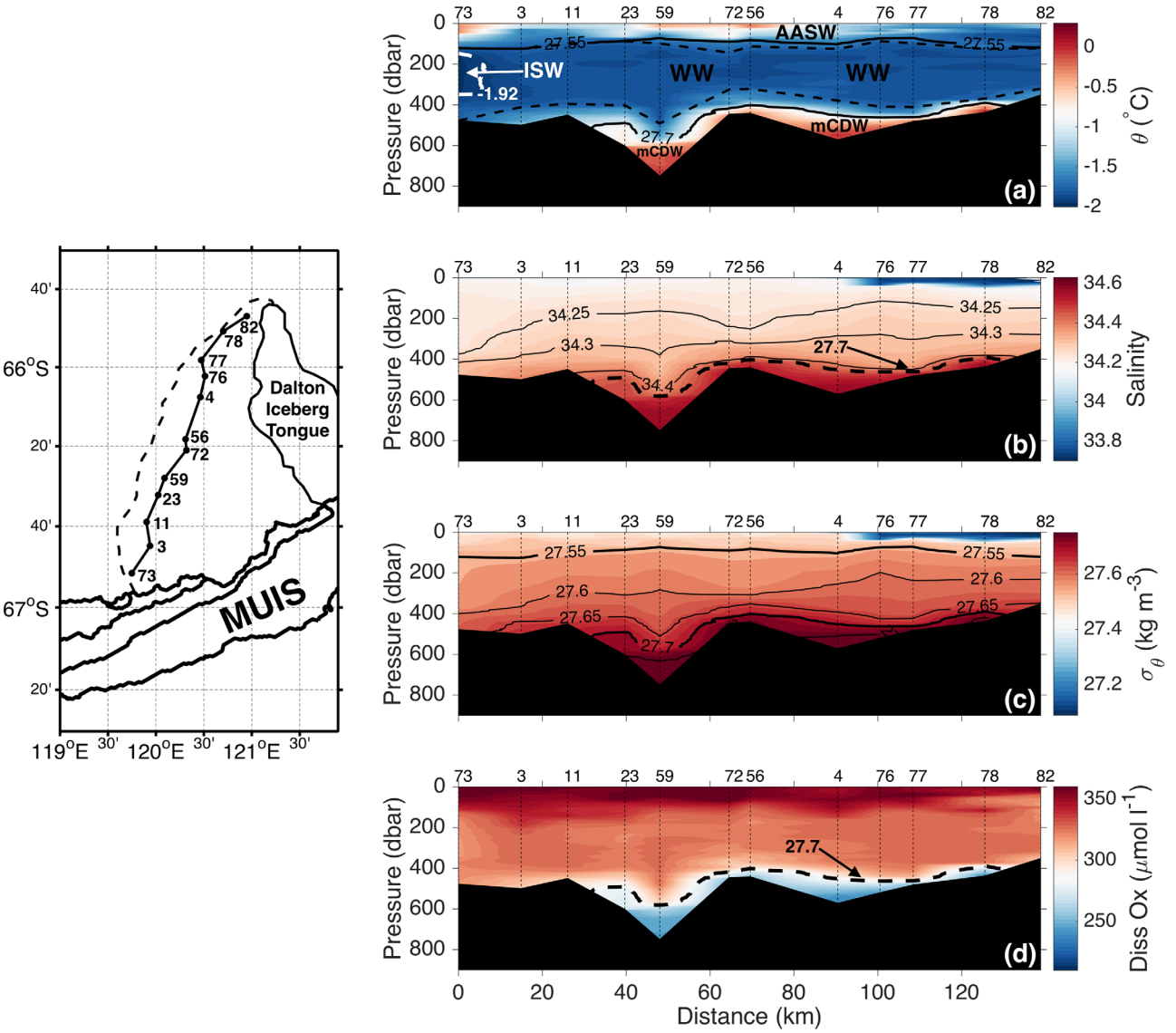

Figure 2. Meridional section through the Dalton Polynya. (a) Potential temperature θ, (b) salinity, (c) potential density σ_θ, and (d) dissolved oxygen section from the meridional transect shown in Figure 1 and highlighted in the inset map (the dashed black line is the approximate eastern boundary of the area covered by sea ice). CTD stations are indicated by the vertical dashed lines (numbered along the top of the plot). In plot (a) contours of σ_θ are included in black as well as the contour of $\theta = -1.92$°C (Ice Shelf Water) in dashed white, while the black dashed lines indicate the top and the bottom of the Winter Water (WW) layer. The modified Circumpolar Deep Water (mCDW) is found below the contour of $\sigma_\theta = 27.7$ kg m^{-3} (dashed black line in the plots (b) and (d)) and the Antarctic Surface Water (AASW) above the contour of $\sigma_\theta = 27.55$ kg m^{-3}.

Table 1. Classification of the Water Masses

Water Mass	σ_θ (kg m^{-3})	θ (°C)
AASW	$\sigma_\theta < 27.55$	
WW	$27.55 < \sigma_\theta < 27.7$	$-1.92 < \theta < -1.75$
ISW	$27.55 < \sigma_\theta < 27.7$	$\theta < -1.92$
mCDW	$\sigma_\theta > 27.7$	

water mass that is the product of winter convection, excluding water from the seasonal and main pycnocline, we restrict our definition of WW to subsurface water in the σ_θ range 27.55–27.7 kg m^{-3} and potential temperature range −1.92 to −1.75°C.

The final water mass found during the survey is Ice Shelf Water (ISW), which results from mixing between glacial meltwater from ice-shelf basal melt and ambient shelf water masses. ISW is distinguished from the other water masses by temperatures colder than the surface freezing point, reflecting basal melting at depth. We define ISW as water colder than −1.92°C, which corresponds roughly to the local subsurface freezing point at 50 dbar; it is unlikely that water colder than this value is the result of the interaction with the atmosphere

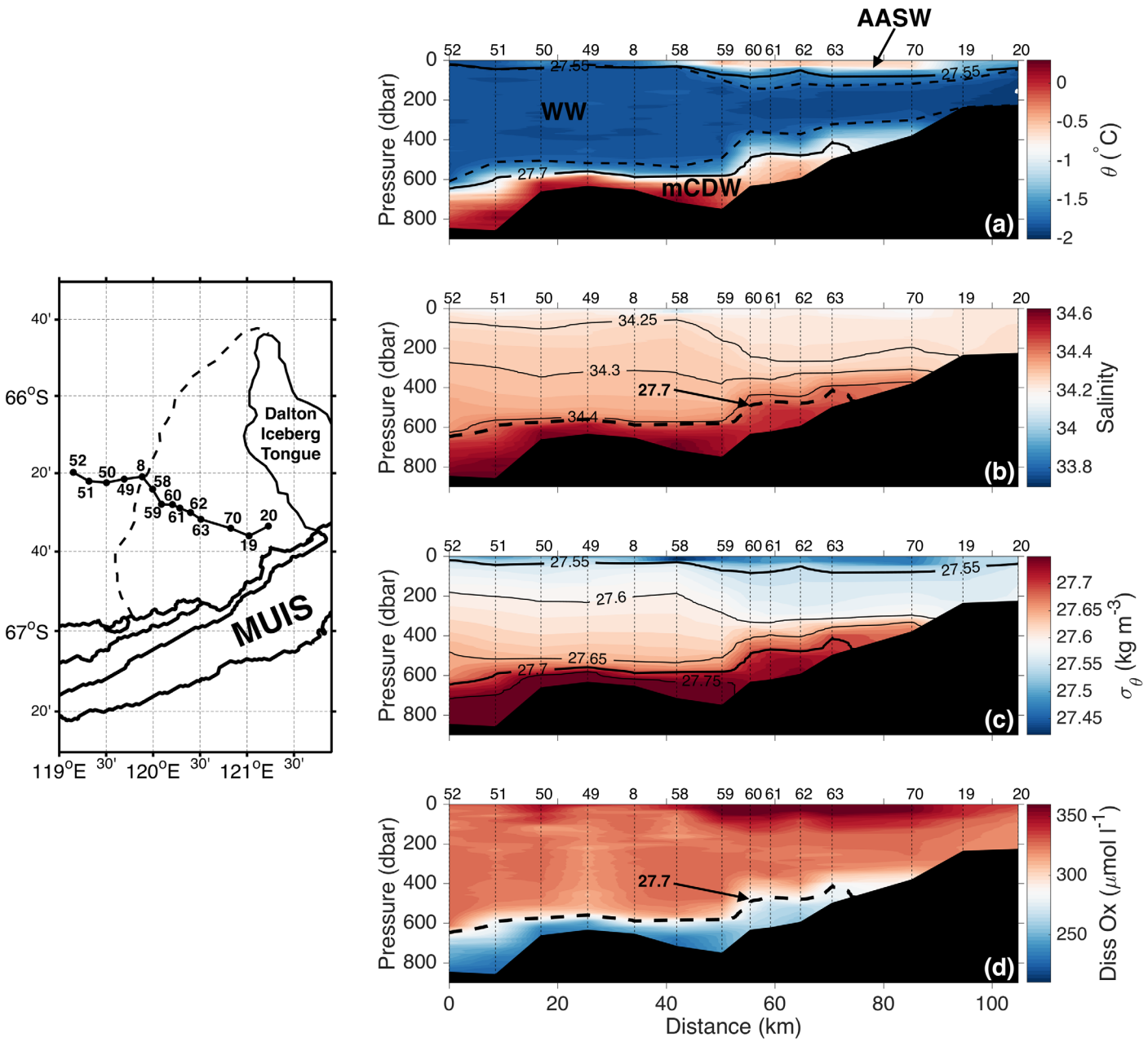

Figure 3. Zonal section through the Dalton Polynya. As in Figure 2 but for the zonal transect shown in Figure 1 and in the inset map.

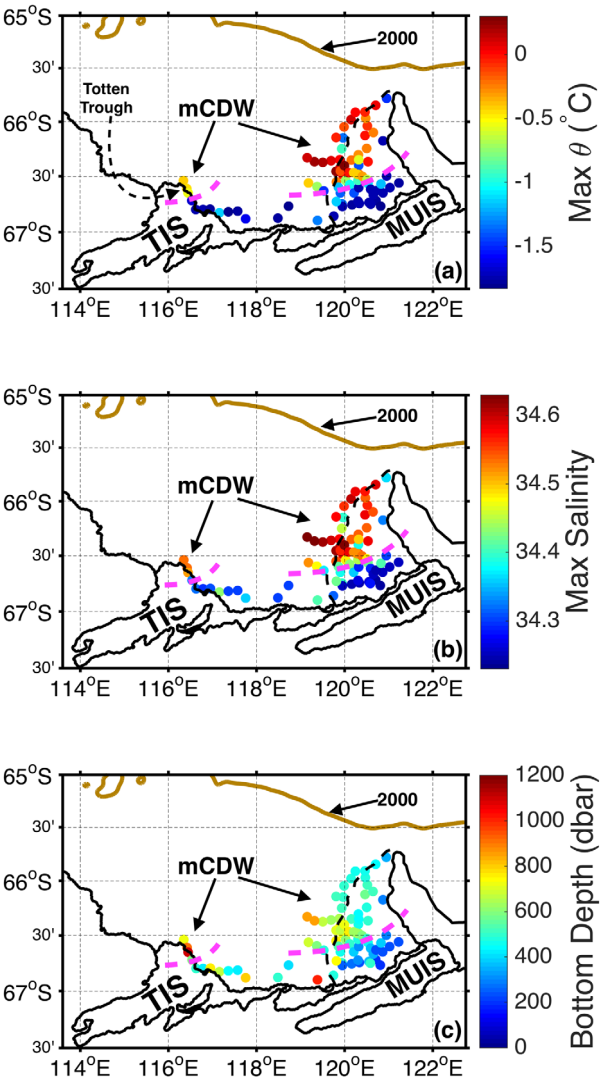

Figure 4. Maximum property values. (a) Maximum potential temperature θ and (b) salinity beneath the summer mixed layer. The brown line is the 2000 m isobath (showing the approximate location of the continental slope) and the black dashed line the approximate eastern boundary of the area covered by sea ice. The magenta dashed lines are the mCDW southern boundary. (c) Bottom depth (dbar).

during the winter [*Orsi and Wiederwohl*, 2009]. ISW is found near the coast (see Figure 2a) in the same density range as the WW (27.55 kg $m^{-3} < \sigma_\theta < 27.7$ kg m^{-3}). The classification of the relevant water masses found on the shelf of Sabrina Coast is summarized in Table 1.

3.2. Spatial Distribution of Water Properties

We divide the domain into two regions in order to analyze the spatial variability of the water properties: the DP (red points in Figure 1) and the ice front, which includes the stations closest to the TIS and MUIS calving front (blue and green points in Figure 1, respectively). A recent airborne survey revealed the presence of an inland cavity (highlighted in Figure 1) that connects the main trunk of the TIS with the adjacent fringing ice shelf [*Greenbaum et al.*, 2015]. In order to include this cavity in the definition of the TIS, we extend the eastern boundary of this ice shelf to 118°E. We define the floating ice shelves between 118°E and 122.5°E as the MUIS. Furthemore, for simplicity, the DP group includes stations located in sea ice west of the actual polynya and the ice-front group includes stations collected along the narrow part of the coast where the ice front is not floating but grounded on bedrock (between the main trunk and the subsidiary part of the MUIS, according to Bedmap2).

3.2.1. Dalton Polynya

The mCDW is widespread at depth in the DP and its southward spreading is steered by bathymetry. The meridional transect through the DP indicates that mCDW is found below 400–500 m across most of the section (Figure 2). However, closer to the ice front, the deepest water gets colder as the bottom shoals. Near the MUIS, the sea floor rises to about 500 m and the bottom water temperature is almost at the surface freezing point. The distributions of salinity and dissolved oxygen are closely related to potential temperature. The warmest mCDW is also the most saline and lowest in oxygen, while the cooler bottom water near the coast is fresher and higher in oxygen. A similar pattern is found in the zonal direction (Figure 3). In the south-eastern sector of the polynya, mCDW is not found in the shallow waters (<300 m) near the coast. Moving north-westward, the temperature at the bottom increases as the bottom deepens. At station 63, where the sea floor is about 500 m deep, the mCDW signal reappears. In both transects, isopycnals follow the slope of the sea floor, implying that mCDW is steered by bathymetry.

To help visualize the spreading of mCDW on the shelf, we show the spatial distribution of the warmest and saltiest water found beneath the summer mixed layer (Figures 4a and 4b). The warmest (0.3°C), saltiest (34.63), and lowest oxygen (~230 μmol L^{-1}, Figure 3d) mCDW is located in the western part of the DP. In the north, the mCDW is slightly cooler and fresher. Approaching the coast in the DP, the bottom shoals (Figure 4c) and the deep water

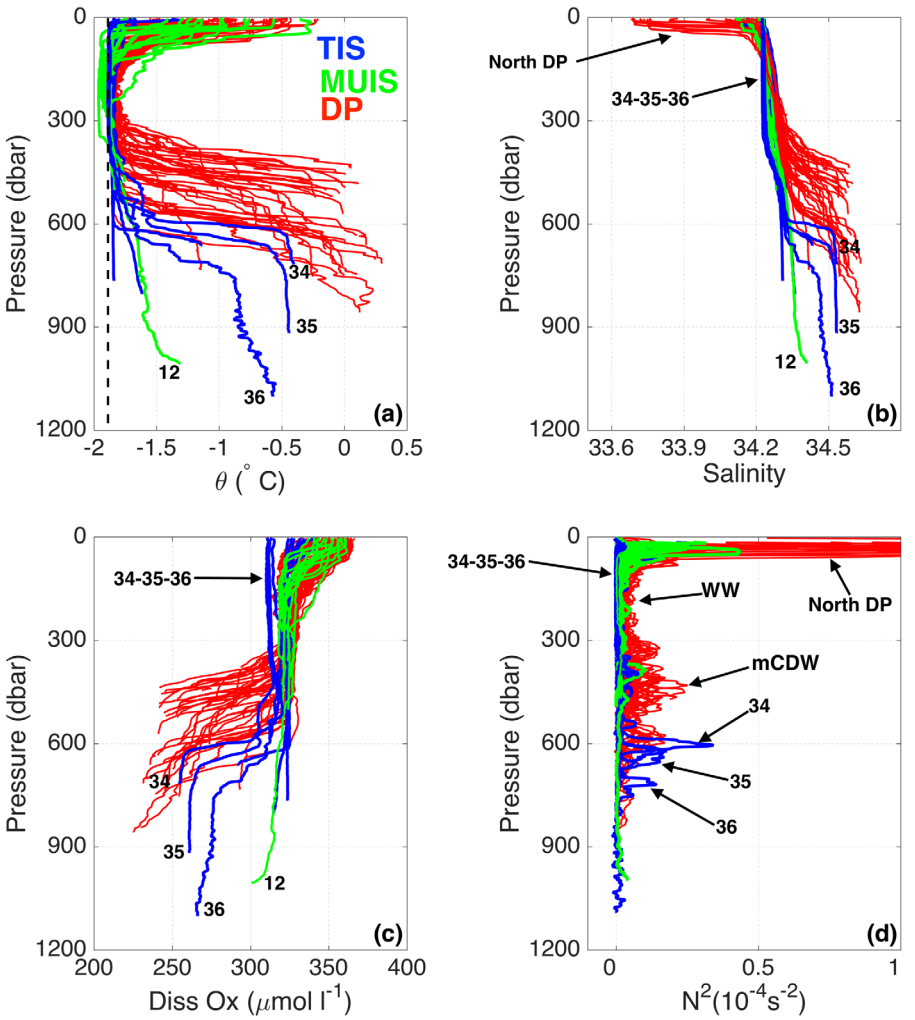

Figure 5. Vertical profiles. (a) Potential temperature θ, (b) salinity, (c) dissolved oxygen, and (d) N^2 (square of the Brunt-Väisälä frequency) profiles from DP (red), MUIS (green), and TIS (blue) calving fronts. The westernmost profiles (34, 35, and 36) are labeled, as well as station 12 where a deep trough is found at the MUIS calving front. Overlaid in black in Figure 5a is the surface freezing temperature profile for a salinity of 34.4, representative of the domain. N^2 has been smoothed with a vertical running mean over 20 dbar.

becomes cooler and fresher. The magenta dashed line indicates the southern boundary of the mCDW core. As expected, this boundary corresponds roughly to where the bathymetry becomes shallower than 500 m. In the DP, south of this line, the bottom layer gets progressively cooler and fresher until any trace of mCDW vanishes and the WW extends to the bottom.

The mCDW layer in the polynya is characterized by strong vertical gradients: temperature and salinity increase with depth, while the oxygen content diminishes (Figures 5a–5c). The strong salinity gradient, and the consequent strong density gradient, indicates that mCDW is more stable than the overlying WW (Figure 5d). The pycnocline deepens from ∼400 m in the shallower northern region to ∼600 m in the deeper water in the west, resulting in a 100–200 m thick bottom layer in both regions (Figures 2 and 3) that shows small spatial variability of the water properties (Figure 4).

Above the mCDW, the WW fills most of the water column, occupying a 300–500 m thick layer, depending on the bathymetry. The WW is cold (∼−1.8°C), relatively fresh (salinity ∼34.3), and higher in oxygen (∼330 μmol L^{-1}) than the underlying mCDW. In contrast to their vertical homogeneity, the WW properties show a large horizontal variability. First, the WW temperature near the coast is ∼0.1°C lower than in rest of the polynya (Figure 6a, note that we included both WW and ISW in order to capture the product of the interaction between ice and ocean on intermediate waters). Moreover, the WW salinity substantially decreases

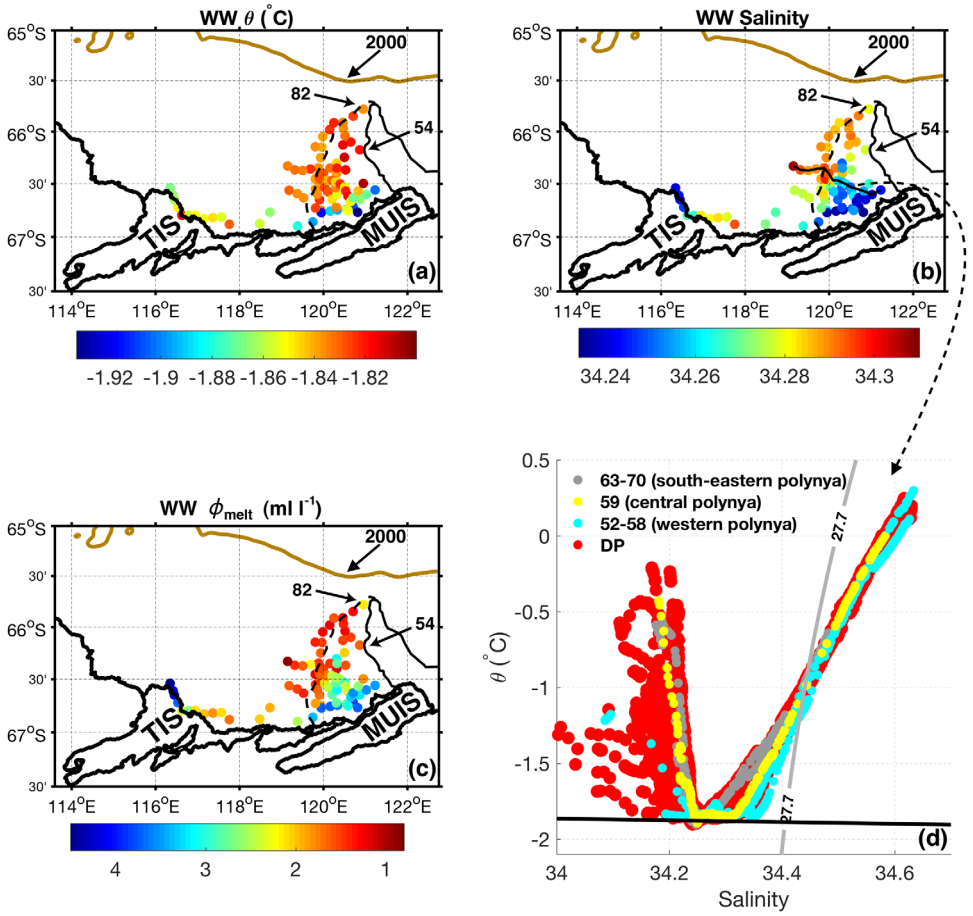

Figure 6. WW Properties. (a) Mean potential temperature θ, (b) salinity, (c) basal meltwater fraction ϕ_{melt} of Winter Water, WW. The brown line indicates the 2000 m isobath (showing the approximate location of the continental slope) and the black dashed line is the approximate eastern boundary of the area covered by sea ice. Note that the Ice Shelf Water is included in the WW properties. We calculate the vertical average above the lower limit of WW and below the upper limit of WW or the maximum depth where the ϕ_{melt} estimate is contaminated by surface processes, whichever is deeper. (d) Potential temperature θ versus salinity from DP. The red points indicate data from all the profiles collected in the DP, while grey points (stations 63 and 70) are indicative of the south-eastern DP, yellow points (station 59) of the central DP and the light blue points (stations 52 and 58) of the western DP. These stations are chosen along the zonal transect highlighted in Figure 6b and in Figure 3. For the exact location of these stations see Figure 1. The grey line is the contour of $\sigma_\theta = 27.7$ kg m^{-3} (upper boundary of mCDW) and the black line is the surface freezing point.

approaching the coast with values up to 0.05–0.06 lower than in the western/northern polynya (Figure 6b). This gradual freshening is reflected in the downward tilting of isohalines and isopycnals toward the coast (clearly seen along the 34.25 isohaline, see Figures 2b and 3b). Few measurements have been collected near the Dalton Iceberg Tongue (stations 54 and 82, see Figure 1 for location). Here the WW has similar temperatures but slightly lower salinity values (∼0.01–0.02) compared to further west (Figures 6a and 6b).

The shift to cooler and fresher values near the coast is not restricted to the WW layer, but also observed in the underlying pycnocline. This behavior is clearly seen by following the properties of the pycnocline on a θ-S diagram. In the zonal line shown in Figure 3, there is a shift of the pycnocline (mCDW-WW mixing line) toward the bottom left (cooler and fresher) corner of the diagram approaching the coast (Figure 6d). Our results therefore show that most of the water column (WW layer and the underlying pycnocline, to a depth of 300–400 m) is affected by cooling and freshening near the coast.

Finally, the upper part of the water column is occupied by the AASW. The AASW varies strongly across the region reflecting the absence or presence of sea ice and whether or not sea-ice melt has occurred. The polynya was completely ice free in November and during the first weeks of December 2014 [*Scambos et al.*, 1996], just before the survey, allowing warming of surface waters in early summer. In the polynya, a ∼50 m thick layer of relatively warm (up to ∼−0.2°C) AASW overlies the WW. Outside the polynya, sea ice was present

prior to and during the survey. Here AASW is essentially absent and the WW layer extends to the surface. In the northern polynya we observe a fresh (salinity < 34) surface layer due to sea-ice melting that occurred in the last days of the survey (Figures 2b and 5b). This surface layer is highly stratified ($N^2 \sim 10^{-4}$ s^{-2}, Figure 5d) due to the strong input of freshwater at the surface. Because of the strong stratification, the observed freshwater input due to melting of sea ice does not affect the underlying WW. In fact the WW properties (e.g., salinity) are similar, here, to the western polynya, where sea-ice melting did not occur (Figures 6a and 6b).

3.2.2. Ice Front

The ice-front section indicates that relatively warm (~ -0.4°C), salty ($\sim$34.53), and oxygen-poor ($\sim$260 μmol L^{-1}) mCDW reaches the western sector of the TIS calving front (Figure 7). Here the deep water is colder and fresher than the mCDW found in the DP, but still 2–2.2°C above the in situ freezing temperature. Direct velocity measurements from a Lowered Acoustic Doppler Current Profiler (LADCP) confirm that the warm water is flowing strongly into the cavity through the Totten Trough at stations 35 and 36 [*Rintoul et al*., 2016]. Because the warm water at depth is flowing into the cavity, the interleaving observed below $\sim$800 m at station 36 (Figures 5a–5c) is a surprise. The interleaving signal (e.g., temperature variations of 0.05–0.1°C over tens of meters) is large relative to the error in the measurement. The interleaving at depth might indicate mixing with a small amount of glacial meltwater that detrains from the ice-shelf base at depth. With the exception of the weak interleaving, the mCDW at the western TIS front forms a relatively homogeneous deep layer (Figure 5), in contrast to the well-stratified mCDW found in the DP. The homogeneity and relatively cool temperature of the mCDW at the ice front likely reflects the presence of a sill that restricts access of water warmer than -0.4°C to the TIS cavity.

Above the mCDW layer, the θ-S diagram shows that the pycnocline (mCDW-WW mixing line) observed at stations 34, 35, and 36 in the western sector of the TIS front departs from the trend observed in the polynya (Figure 8a). This shift toward fresher (and cooler) values is a signal of addition of freshwater. Other measurements from the TIS calving front (station 41) overlap the DP trend, confirming that this shift is not due to different ambient water properties on the Sabrina Coast continental shelf, but rather the addition of freshwater along the western ice front. The O_2-S diagram confirms the strong departure of the mCDW-WW mixing line from the ambient trend (Figure 8b).

The WW at the western TIS front is fresh ($\sim$34.25), low in oxygen ($\sim$300 μmol L^{-1}), and very weakly stratified compared to the WW found elsewhere on the shelf (Figures 5b–5d), including further east along the calving front (Figure 7). The low oxygen and salinity are responsible for the bump observed in the O_2-S plot (Figure 8b) and reflects an outflow driven by upwelling of a mixture of glacial meltwater and mCDW from the cavity. Further east along the TIS calving front there are no indications of any substantial fresh outflows. At the eastern TIS calving front, the deep water that can reach the inland cavity hypothesized by *Greenbaum et al*. [2015] is cooler than -1.1°C (stations 41, 42, 43, and 33, Figure 7a), significantly colder than in the Totten Trough.

In contrast to the TIS, the WW reaches the bottom along most of the MUIS calving front. Only one deep ($\sim$1000 m) trough at station 12 shows relatively warm (~ -1.3°C) and oxygen-poor ($\sim$300 μmol L^{-1}) deep water (Figures 7a and 7d). Near this trough the WW is replaced by ISW ($\theta < -1.92$°C) at depths shallower than the ice draft, between 100 and 400 m below the sea surface (Figure 7a). The ISW is fresher ($\sim$34.25) and lower in oxygen ($\sim$320 μmol L^{-1}) than the surrounding WW (salinity $\sim$34.3 and oxygen $\sim$330 μmol L^{-1}) (Figures 7b and 7d). The ISW properties are also clear in the θ-S and O_2-S diagram by the bumps below the surface freezing point and below the WW-mCDW mixing line trend, respectively (Figure 8). To summarize, we observe at the MUIS ice front relatively warm water at depth that can access the cavity through a deep trough, coincident with low oxygen ISW at depths shallower than the ice draft. These findings indicate that the ISW results from basal melt driven by deep intrusions of relatively warm and low oxygen water into the MUIS cavity, similar to the TIS. Low oxygen ISW is found not only in front of the ice shelf, but along most of the coast where the ice is grounded, up to 75 km east of the deep trough located at station 12 (Figure 7).

3.3. Distribution of Glacial Meltwater

In this section, we quantify the glacial meltwater concentration in the water column throughout the survey area. Glacial meltwater is produced by ice-shelf/iceberg basal melting and surface runoff. The contribution from surface runoff is negligible since summer air temperature in the interior of the East Antarctic Ice Sheet and on the Sabrina Coast is well below freezing and therefore surface melting can be ignored [*Fyke et al*., 2010; *Picard and Fily*, 2006]. For simplicity, we refer to glacial meltwater produced by basal melt of ice

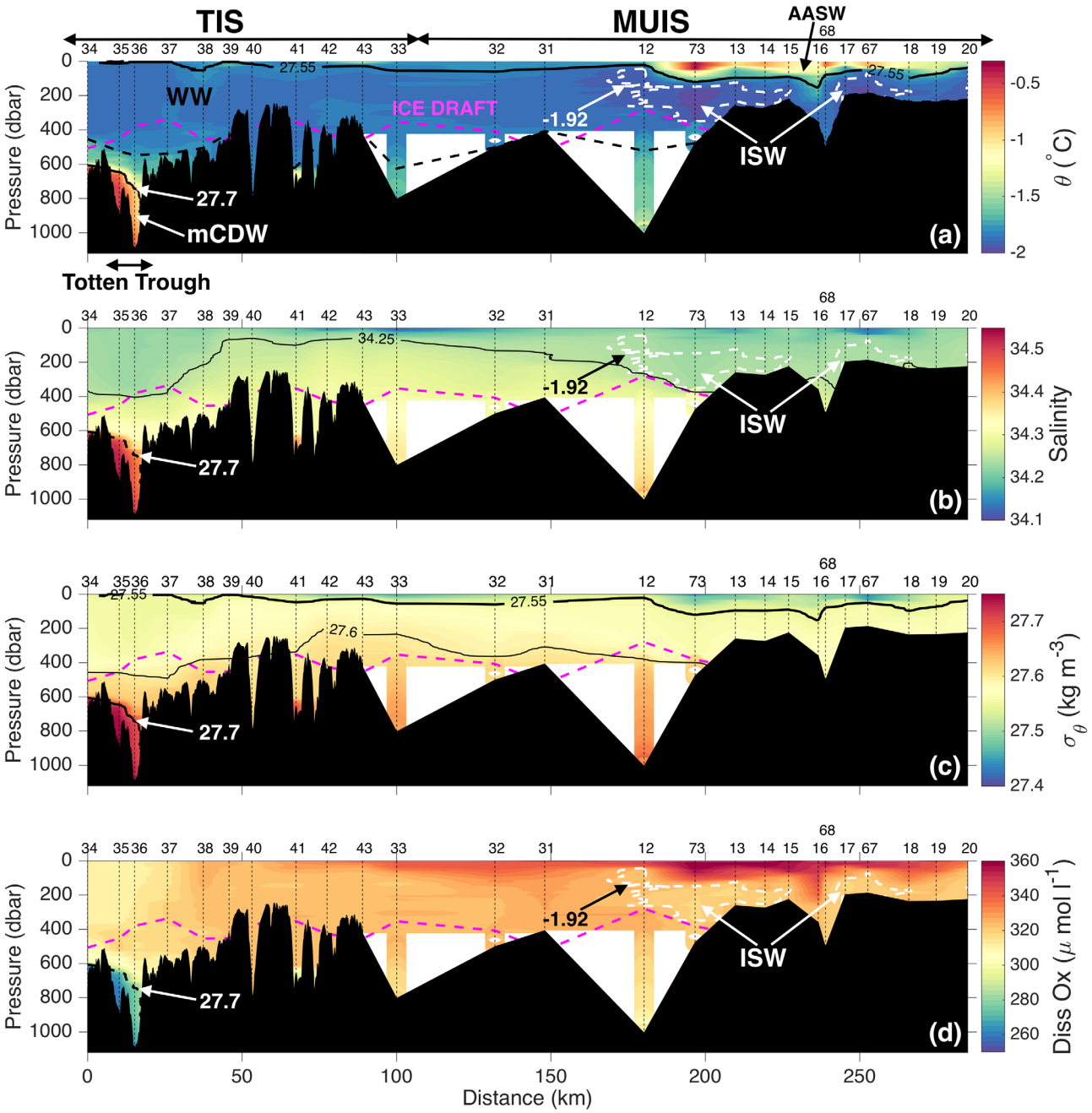

Figure 7. Ice-front section. As Figure 2 but for the calving front of TIS and MUIS (blue and green dots in Figure 1, respectively). Note that the upper limit of the WW layer roughly overlaps the potential density contour of 27.55 kg m^{-3} and therefore is not labeled. From stations 34 to 43, we use the bathymetry data collected during the voyage. East of station 43, the coverage does not provide high resolution bathymetry on a straight line between the stations and therefore only the depth at each station is used. Along the MUIS calving front, where the distances between stations are large, we do not interpolate below the deepest common depth at each station pair. The magenta dashed line indicates the approximate draft of the ice shelf near the calving front. From station 34 to station 42, the draft is interpolated from airborne measurements [*Greenbaum et al*., 2015], while from stations 43 to 15, the draft is obtained from Bedmap2 estimate of ice thickness [*Fretwell et al*., 2013]. East of station of 15 the ice front is grounded, according to Bedmap2.

shelves and icebergs as basal meltwater. We use the method of *Jenkins* [1999] to estimate the basal meltwater fraction ϕ_{melt} from potential temperature, salinity, and dissolved oxygen. This method has been successfully applied both at the calving front of several ice shelves [e.g., *Jenkins and Jacobs*, 2008; *Jacobs et al*., 2011] and on the continental shelf further offshore [e.g., *Randall-Goodwin et al*., 2015]. Estimates of ϕ_{melt} using this technique have been found to be consistent with studies using other tracers such as neon and helium [*Jenkins and Jacobs*, 2008; *Kim et al*., 2016].

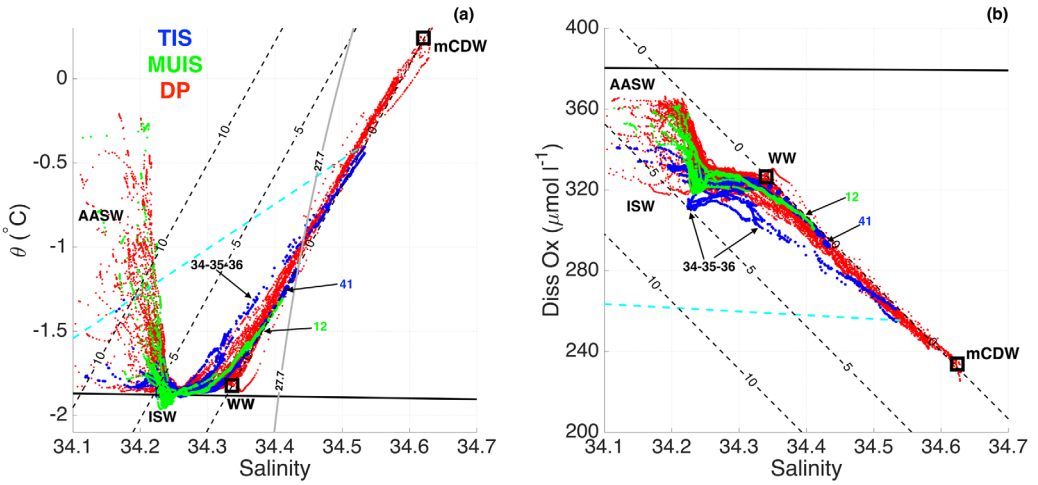

Figure 8. θ-S/O_2-S diagram. (a) Potential temperature θ versus salinity and (b) dissolved oxygen versus salinity from DP (red), MUIS (green), and TIS calving fronts (blue). The cyan dashed line is the mixing line (in the θ-S plot also known as Gade Line) between the warmest mCDW found in front of TIS and pure glacial meltwater, while the black dashed lines indicate contours of basal meltwater fraction (ml L^{-1}). The square boxes refer to the ambient properties used to calculate the basal meltwater fraction. The black line is the surface freezing point in Figure 8a and the surface of saturation for water at the surface freezing point in Figure 8b. The westernmost profiles (34, 35, and 36) are labeled. The grey line in plot (a) represents the surface of $\sigma_\theta = 27.7$ kg m^{-3} (upper boundary of mCDW). AASW, Antarctic Surface Water; ISW, Ice Shelf Water; mCDW, modified Circumpolar Deep Water; and WW, Winter Water.

The method of *Jenkins* [1999] can be used to estimate the meltwater concentration relative to the ambient water. In the simple case where basal meltwater is added to a single ambient water mass, we can write a conservation equation for a conservative tracer χ:

$$\chi_{obs} = (1-\phi_{melt})\chi_{wm} + \phi_{melt}\chi_{melt} \tag{1}$$

where χ_{obs} is the measured tracer property, and χ_{wm} and χ_{melt} are the tracer properties of the ambient water mass and basal meltwater, respectively. From equation (1), it follows that ϕ_{melt} can be estimated as:

$$\phi_{melt} = \frac{\chi_{obs} - \chi_{wm}}{\chi_{melt} - \chi_{wm}} \tag{2}$$

If the ambient water is a mixture of two water masses ("wm1" and "wm2"), we can write conservation equations for two conservative tracers χ^1 and χ^2:

$$\begin{cases} \chi^1_{obs} = (1-\phi_{melt}-\phi_{wm2})\chi^1_{wm1} + \phi_{melt}\chi^1_{melt} + \phi_{wm2}\chi^1_{wm2} \\ \chi^2_{obs} = (1-\phi_{melt}-\phi_{wm2})\chi^2_{wm1} + \phi_{melt}\chi^2_{melt} + \phi_{wm2}\chi^2_{wm2} \end{cases} \tag{3}$$

where ϕ_{wm2} represents the concentration of the water mass "wm2". On the Sabrina Coast continental shelf, we can use observations of two conservative tracers to solve the system of equations (3) beneath the summer mixed layer, where the ambient water is a mixture of mCDW ("wm1") and WW ("wm2"). After some simple algebra, we obtain that the basal meltwater fraction is given by:

$$\phi_{melt} = \frac{\left(\chi^2_{obs} - \chi^2_{mCDW}\right) - \alpha\left(\chi^1_{obs} - \chi^1_{mCDW}\right)}{\left(\chi^2_{melt} - \chi^2_{mCDW}\right) - \alpha\left(\chi^1_{melt} - \chi^1_{mCDW}\right)} \tag{4}$$

where $\alpha = \frac{\left(\chi^2_{WW} - \chi^2_{mCDW}\right)}{\left(\chi^1_{WW} - \chi^1_{mCDW}\right)}$. This derivation of equation (4) differs from that of *Jenkins* [1999], but gives the same result.

Using potential temperature, salinity, and dissolved oxygen as conservative properties below the surface layer, three different estimates of ϕ_{melt} can be obtained based on three possible pairs of these tracers (θ-S, θ-O_2, and O_2-S). The values corresponding to the warmest, saltiest, and lowest oxygen water found on the shelf ($\theta = 0.3$°C, $S = 34.63$, and $O_2 = 230$ μmol L^{-1}) are taken as representative of the mCDW core. The WW end member ($\theta = -1.8$°C, $S = 34.34$, and $O_2 = 327$ μmol L^{-1}) is defined by the saltiest WW found in the domain [*Randall-Goodwin et al.*, 2015].

The temperature of pure glacial meltwater θ_{melt} can be extrapolated from the so-called Gade Line which describes the mixing line in θ-S space between pure glacial meltwater and the oceanic water source [*Gade*, 1979; *Jenkins and Jacobs*, 2008]:

$$\theta_{melt} = \theta_f - \frac{L}{c_w} - \frac{c_i}{c_w}(\theta_f - T_i) \tag{5}$$

where θ_f is the freezing point temperature at the ice-shelf base and depends on salinity and pressure; L is the latent heat of ice fusion (3.35×10^5 J kg^{-1}); c_W and c_i are the specific heat capacity of seawater and ice (4000 and 2010 J kg^{-1} C^{-1}, respectively) and, T_i is the mean ice temperature of ice shelves and icebergs. No measurements are available on the Sabrina Coast to estimate the latter quantity. We assume T_i to be -15°C in agreement with the ice temperature measured at the Amery Ice Shelf in East Antarctica [*Herraiz-Borreguero et al*., 2013]. The oceanic source can be any water parcel found along the mCDW-WW mixing line. Considering a typical ice draft in TIS of 500 m [from Bedmap2, *Fretwell et al*., 2013] and a salinity of 34.4 representative of the domain, we find that θ_{melt} is about -92°C, comparable to estimated values in Amundsen ice shelves [e.g., *Hellmer et al*., 1998; *Jenkins and Jacobs*, 2008]. Note that ϕ_{melt} is not very sensitive to the estimated θ_{melt} and hence to the values of the freezing point temperature or ice temperature selected.

The oxygen content of pure glacial meltwater is estimated from the empirical relation obtained by *Martinerie et al*. [1992] between oxygen concentration of the ice (and therefore of pure glacial meltwater) and the elevation where the ice is formed. According to this empirical law and considering that the elevation of the catchment that feeds the TIS and MUIS is around 2000–3000 m [*Fretwell et al*., 2013], we obtain a value around 900 μmol L^{-1} for the dissolved oxygen content of pure glacial meltwater (note that ϕ_{melt} is not particularly sensitive to this value). The mixing line between the warmest, saltiest, and lowest oxygen mCDW found in front of TIS and pure glacial meltwater in θ-S (Gade Line) and O_2-S space is shown in Figure 8 by the cyan line. The shift of the pycnocline at the western TIS front toward the Gade Line supports the hypothesis that basal melt supplies a source of freshwater.

Following *Jenkins and Jacobs* [2008], we regard O_2-S as the most reliable pair to calculate ϕ_{melt}. When the difference between the basal meltwater fraction calculated with the other two property pairs (θ-S and θ-O_2) is larger than 3.5 ml L^{-1}, we disregard the calculation because it is likely affected by interaction with the atmosphere. Beneath this level, the uncertainty in the estimated ϕ_{melt} is mainly due to the deviation from linear mixing between WW and mCDW [*Jenkins and Jacobs*, 2008]. In order to provide a quantitative estimate of this uncertainty, we calculate the difference between ϕ_{melt} estimated as described above and ϕ_{melt} calculated considering the freshest form of WW found on the shelf ($S = 34.27$). We perform this calculation for every set of in situ θ, S, and O_2. In other words, we investigate the impact of a shifted mixing line on the calculation of ϕ_{melt}. Although this shift is not observed, it provides an upper bound on the uncertainty, as it represents the maximum plausible departure from the observed mixing line. Neglecting negative values of ϕ_{melt}, which are not physical and arise from shifting the mixing line, the average difference between the two calculations is smaller than 2 ml L^{-1}. We then treat 2 ml L^{-1} as the upper bound on the uncertainty of ϕ_{melt}.

The basal meltwater fraction agrees well with the observed water properties (Figure 9). Where there are inflows of deep and warm water, as in the Totten Trough and in the MUIS trough at station 12, the basal meltwater content is small. Where there are fresh outflows, ϕ_{melt} increases. The highest basal meltwater content is found in the outflow along the western TIS calving front with values up to 5 ml L^{-1}. The ISW also has a strong meltwater signature, as expected, with maximum values of ϕ_{melt} up to 4 ml L^{-1}. The meltwater content of the outflow is higher at the TIS calving front than at the MUIS front. This result is consistent with the observation that warmer mCDW reaches the TIS cavity, driving higher rates of basal melt.

The influence of the basal meltwater input is not limited to the TIS and MUIS calving front. As noted above, the WW salinity decreases near the coast in the polynya (Figure 6b). The basal meltwater concentration shows a similar distribution, with values of 1-1.5 ml L^{-1} in the western/northern polynya increasing to values in excess of 3 ml L^{-1} in the southern polynya (Figure 6c). The similarity between the two patterns suggests the low salinity of WW in the southern polynya reflects dilution by basal meltwater. Near the Dalton Iceberg Tongue, at stations 54 and 82, the meltwater fraction in WW is about 1.5–2 ml L^{-1} (Figure 6c), a relatively small concentration considering the estimated uncertainty on ϕ_{melt} of 2 ml L^{-1}. The low meltwater concentration near the Dalton Iceberg Tongue is in agreement with the small decrease in salinity there

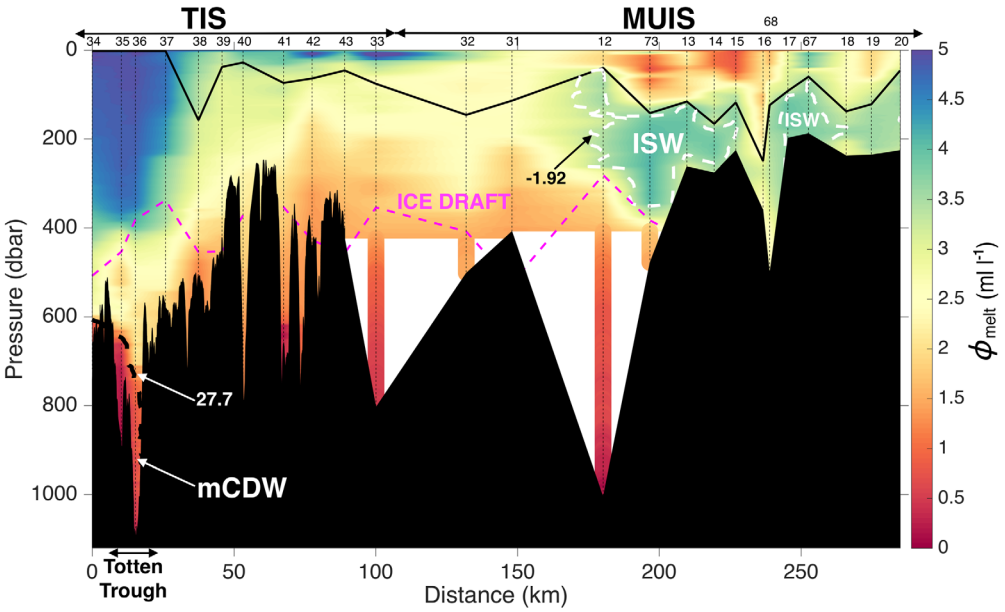

Figure 9. Basal Meltwater Fraction. Vertical section of the basal meltwater fraction ϕ_{melt} (ml L^{-1}) in front of TIS and MUIS. The surface of $\sigma_\theta = 27.7$ kg m^{-3} (upper boundary of mCDW) is indicated by the dashed black line, while the magenta dashed line represents the ice draft, as in Figure 7. The black line is the maximum depth where surface contamination is likely to affect the calculation of ϕ_{melt}. $\theta = -1.92$°C contours (Ice Shelf Water) are in dashed white.

compared to that observed in the southern polynya. This implies that the input of basal meltwater from Dalton Iceberg Tongue is relatively small.

4. Discussion

Our observations show that relatively warm mCDW is widespread below 500 m on the continental shelf of the Sabrina Coast. Fresh WW overlies the saline mCDW. No DSW was observed on the continental shelf, suggesting that winter convection was too weak to erode the stratification and produce water dense enough to mix with the mCDW. The distribution of mCDW properties can be explained largely in terms of bathymetry. The warmest mCDW is found in the deep area on the western side of the polynya (it is possible that even warmer waters might be found further west). Southward shoaling of the bottom prevents the mCDW from reaching the coast in the polynya; relatively warm water can reach the TIS and MUIS cavities only through localized troughs. The warmest mCDW observed on the shelf is ~0.7°C warmer than the warmest water reaching the TIS and ~1.6°C warmer than the water reaching the MUIS. A sill or other bathymetric barrier in an area not covered by our survey presumably prevents the warmest water found on the shelf from reaching the TIS and MUIS cavities. With the exception of airborne surveys that cover the TIS cavity and surroundings, the only available bathymetric information on the shelf is derived from satellite altimetry measurements [e.g., *Smith and Sandwell*, 1997], which do not resolve small-scale features such as sills or narrow troughs. Our results highlight the need for high resolution bathymetric surveys to identify the controls on delivery of ocean heat to the ice shelves and for use in model simulations of warm water intrusions into the ice-shelf cavities.

Deep water observed at the ice front is cooler than the mCDW observed in the polynya but still about 1°C (at the MUIS) and 2°C (at the TIS) above the local freezing point and therefore sufficiently warm to produce substantial basal melt at depth. *Rintoul et al.* [2016] showed that the ocean heat flux into the TIS cavity was sufficient to account for the rapid basal melt inferred by satellites. Using our extended data set we conclude that the high rate of basal melt inferred at the MUIS is also likely driven by deep intrusions of cooler, but still relatively warm, water.

Input of basal meltwater causes the observed shoreward freshening in the southern DP of the water column above the mCDW. Four lines of evidence support this statement. (1) The distributions of WW salinity and

WW basal meltwater fraction co-vary in the polynya, with substantial freshening and increase in meltwater concentration near the coast. (2) Shoreward shift of the mCDW-WW mixing line toward cooler and fresher values (i.e., toward the mCDW-meltwater mixing line or Gade Line) indicates that the signal of meltwater is detected to 300–400 m depth. (3) Freshening by melting of sea ice is expected to be more intense in the northern side of the polynya than near the coast. (4) The precipitation rate integrated over the southern half of the Dalton Polynya estimated using ERA-Interim (European Centre for Medium-Range Weather Forecasts Interim Re-Analysis) precipitation data [*Dee et al*., 2011] is more than an order of magnitude smaller than freshwater fluxes from basal melt of the nearby MUIS (both the main trunk and the subsidiary part) [*Liu et al*., 2015]. The resolution of the ERA-Interim data does not allow to detect any spatial variability within the polynya. Indeed precipitation could be enhanced near the coast, but given the small magnitude of the integrated precipitation rate, such contribution is likely to be negligible. Freshening by input of glacial meltwater has been also reported in the Amundsen and Bellingshausen seas, where the meltwater signature is widespread on the continental shelf above the mCDW layer [*Wåhlin et al*., 2010; *Kim et al*., 2016; *Randall-Goodwin et al*., 2015; *Zhang et al*., 2016].

The widespread influence of basal meltwater on water properties in the southern polynya suggests there may be multiple sources. In particular, high meltwater concentrations are observed well to the east of the outflow from the MUIS cavity near the deep trough at station 12, whereas we would expect meltwater to be advected westward by the coastal current. One possible source is basal melt from the main trunk of the MUIS that exits the cavity at the calving front east of 121.5°E and is then advected west by the coastal current. Additional channels or cavities may also connect the main MUIS trunk to the DP, providing a pathway for meltwater. Another possible source is submarine melting of icebergs in the Dalton Iceberg Tongue. However, three observations suggest the contribution from the Dalton Iceberg Tongue is less important than that of the MUIS. (1) The weak freshening of WW observed near the iceberg tongue suggests the meltwater input is small. (2) The draft of the grounded icebergs is too shallow (<500 m) to reach the warm mCDW layer and the thermal forcing driving melt is weak. (3) The low oxygen content of ISW found in the south-eastern polynya indicates the melting is driven primarily by mCDW, which does not reach the Dalton Iceberg Tongue (see Figure 4a). Therefore, we speculate that basal melt under the main trunk of the MUIS represents the major source of the basal meltwater found in the DP. If correct, this implies that mCDW is able to access the cavity beneath the main trunk of the MUIS, as also suggested by modeling studies [*Khazendar et al*., 2013; *Gwyther et al*., 2014].

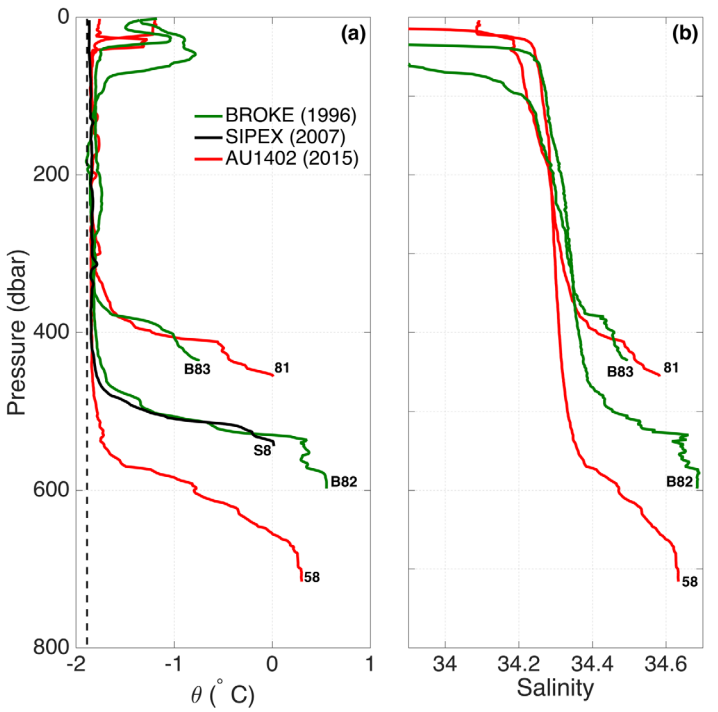

Figure 10. SIPEX-BROKE-AU1402. Vertical profiles of (a) potential temperature θ and (b) salinity from BROKE in 1996 (dark green, stations B82 and B83) and SIPEX in 2007 (black, station S8). For comparison two profiles from the AU1402 expedition in 2015, one from the northern DP (station 81) and one from the western DP (station 58) are overlaid in red. In Figure 10a overlaid in dashed black is the surface freezing temperature for a salinity of 34.4, representative of the domain. The location of the stations is labeled in Figure 1. Salinity data from SIPEX presented a large offset (>0.1) and therefore are not included here.

A comparison with data collected during BROKE and SIPEX reveals that the stratification observed in the polynya in 2015 was similar to that found on the outer shelf in 1996 and 2007 (Figure 10): in each year, relatively warm and saline mCDW was present near the sea floor, overlaid by cold and fresh WW.

(The depth of the pycnocline varies between stations, likely reflecting differences in bottom depth and temporal variability.) Most importantly, none of the profiles collected on the continental shelf shows evidence of DSW. The large salinity (hence density) contrast between fresh WW and saline mCDW stabilizes the water column. This stable stratification persists through winter: the SIPEX profile from later winter 2007 shows a salinity contrast of ~0.3 between WW and mCDW [*Williams et al.*, 2011], similar to summer profiles in 1996 and 2015. Sea-ice production in the DP is low relative to other active Antarctic polynyas [*Tamura et al.*, 2016; *Williams et al.*, 2011] and winter buoyancy loss is apparently insufficient to overcome the stable stratification. Meltwater input contributes to the freshening of the WW, as discussed above, and likely inhibits DSW formation [*Williams et al.*, 2016]. These observations indicate that DSW is not produced in the DP, counter to suggestions from some modeling studies [e.g., *Gwyther et al.*, 2014].

To place our results in a broader context, we compare the ocean properties observed near the Totten Glacier with the Mertz Glacier on the Adélie Coast in East Antarctica and with Pine Island Glacier in Pine Island Bay, West Antarctica (Figure 11). The mCDW is found on the continental shelf in each location, but with different properties. The warmest mCDW is observed in Pine Island Bay (3–4°C above the in situ freezing point). On the Sabrina Coast the mCDW is colder, but still 2–2.5°C above the local freezing point, while on the Adélie Coast the mCDW is less than 1.3°C above the local freezing point. The ocean stratification is qualitatively similar on the Sabrina Coast (see station 52) and in Pine Island Bay (see station 13): beneath the summer mixed layer, cold and fresh WW overlies warm, salty mCDW. In contrast, on the Adélie Coast, the

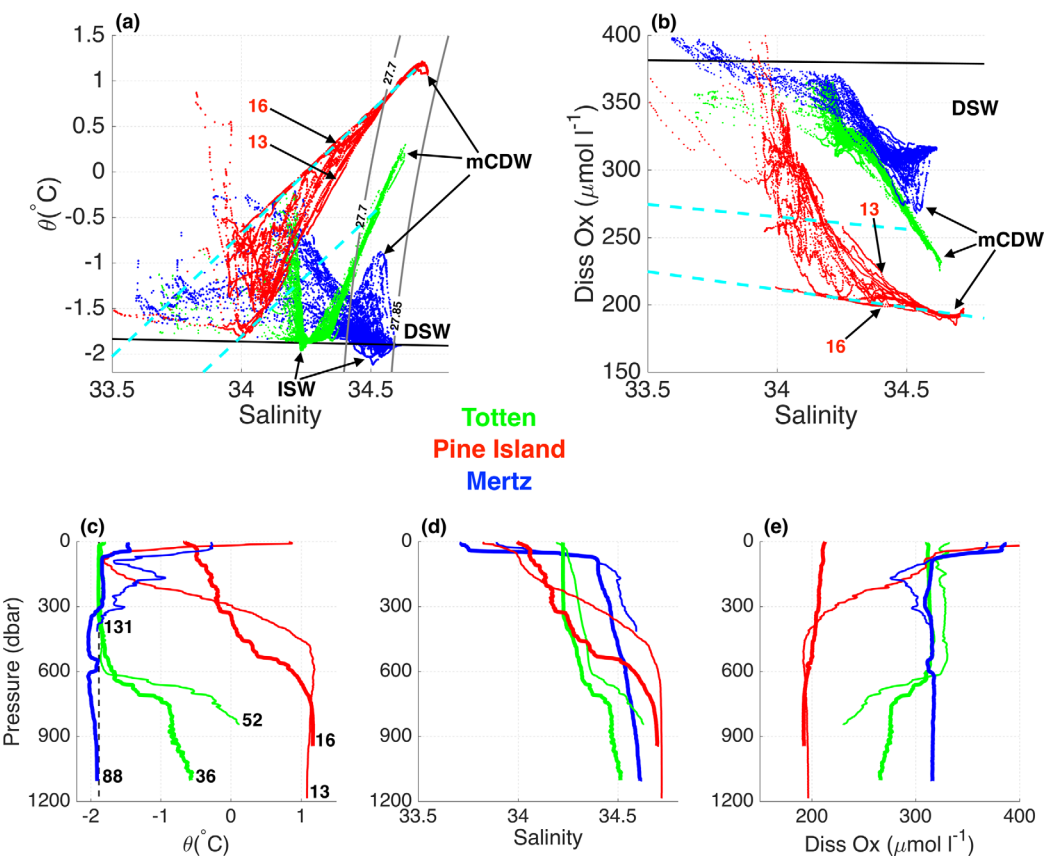

Figure 11. Comparisons between Totten, Mertz, and Pine Island glaciers. (a) Potential temperature θ versus salinity from the shelf in front of Totten (green), Mertz (blue), and Pine Island (red) glaciers. The grey lines represent the surface of $\sigma_\theta = 27.7$ kg m^{-3} (upper boundary of mCDW) and $\sigma_\theta = 27.85$ kg m^{-3} (upper boundary of DSW). The black line is the surface freezing point. The cyan dashed lines are the mixing line between the warmest mCDW found in front of Totten/Pine Island Glacier and pure glacial meltwater. (b) As Figure 11a for dissolved oxygen versus salinity. The black line indicates the surface of saturation for water at the surface freezing point. Vertical profiles of (Figure 11c) theta, (d) salinity, (e) dissolved oxygen showing two profiles for each region. The thin lines are profiles representative of the shelf conditions (station 52/13/131 for Totten/Pine Island/Mertz). The thick lines are profiles representative of the ice-front conditions (station 36/16/88 for Totten/Pine Island/Mertz). The vertical dashed line in plot (c) indicates the surface freezing line for a salinity of 34.3, an intermediate value between the salinity observed at these three locations.

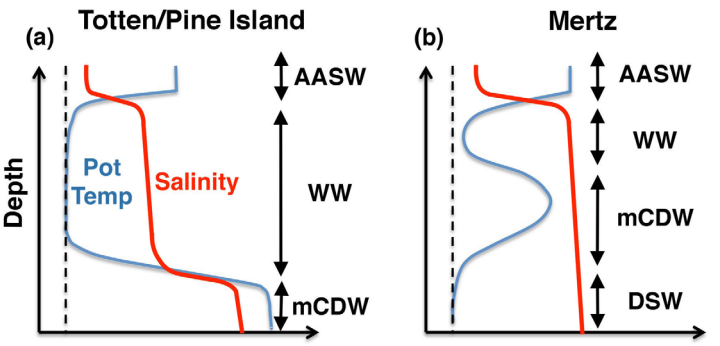

Figure 12. Schematic of the ocean summertime stratification in potential temperature and salinity in front of (a) Totten/Pine Island Glacier and (b) Mertz Glacier. AASW, Antarctic Surface Water; WW, Winter Water; mCDW, modified Circumpolar Deep Water; DSW, Dense Shelf Water.

densest water is cold and oxygen-rich DSW formed during winter [*Shadwick et al.*, 2013]. Above the DSW is the mCDW, a thin layer of cold WW, and the summer mixed layer (see station 131). Intrusions of mCDW are less dense than the DSW on the Adélie Coast, and as a result, the temperature maximum associated with mCDW is found at intermediate depth. In Figure 12, we show a schematic of the different stratification found on the Sabrina Coast, in Pine Island Bay, and on the Adélie Coast.

The difference in stratification found in front of Totten/Pine Island and Mertz glaciers has a large influence on ocean-ice shelf interaction. Near the Mertz Glacier, relatively warm mCDW is found at depths shallower than 300 m and so has limited access to the cavity beneath the Mertz Glacier Tongue. Cold DSW fills the cavity and drives basal melt at depth. The cold and high oxygen ISW at the calving front (e.g., station 88) confirms that high oxygen DSW is the main source of melting under the Mertz Glacier Tongue. The outflow from the Totten and Pine Island cavities is lower in oxygen because the melting source is low oxygen mCDW. A critical difference between the regions is the salinity of the WW: WW is much fresher in Pine Island Bay and on the Sabrina Coast (~34.0 and 34.3, respectively) than on the Adélie Coast (~34.5–34.6). Weak winter salinification results in fresh WW and inhibits convection in West Antarctica and near the Totten Glacier, allowing deep intrusions of warm water into the ice-shelf cavities to drive rapid basal melt. In contrast, strong heat loss and deep convection "protects" most of the East Antarctic outlet glaciers, like Mertz, by limiting the transport of ocean heat to the base of the ice shelves.

The continental shelves on the Sabrina Coast and in West Antarctica share several characteristics: widespread warm mCDW in the bottom layer, weak polynya activity, fresh WW, absence of DSW, high basal melt rates, and widespread glacial meltwater. There are also some important differences. The mCDW is warmer, saltier, and lower in oxygen in Pine Island Bay than on the Sabrina Coast continental shelf. WW is fresher near Pine Island Glacier. The concentration of meltwater in the outflow from the TIS cavity is ~30% of that observed at Pine Island Glacier [*Jacobs et al.*, 2011]. Near Pine Island Glacier, some profiles fall on the mCDW-glacial meltwater mixing line in θ-S and O_2-S space (see station 16 in Figure 11). This is not observed at the Totten calving front, possibly because the outflow has already mixed with WW or because the major outflow from the cavity occurs further west, where fast ice prevented access during the cruise.

A broad trough in front of Pine Island Glacier allows mCDW to reach the cavity along the full width of the calving front, in contrast to the TIS and MUIS, where mCDW inflow is limited to narrow channels. However, bathymetry inside the cavity likely regulates the flux of warm water to the grounding line of Pine Island Glacier [*Dutrieux et al.*, 2014]. Shoaling or deepening of the interface between warm mCDW and cold WW is likely to alter the ocean heat transport to the TIS and MUIS cavity and therefore basal melt, as shown by *Dutrieux et al.* [2014] at Pine Island Glacier. Several processes can influence the depth of the pycnocline on the continental shelf. Variability of mCDW intrusions onto the shelf can modify the thickness of the bottom layer and the depth of the overlying pycnocline [*Thoma et al.*, 2008]. Local changes in winds associated with upwelling/downwelling variability or increased/decreased freshwater fluxes from ice-shelf basal melt can also cause substantial changes in the pycnocline depth [*Padman et al.*, 2012]. Finally, variability in winter convection and thus in the mixed layer thickness can alter the depth at which the pycnocline starts [*St-Laurent et al.*, 2015].

Polynya variability and resulting changes in winter convection may alter heat delivery to the ice-shelf cavities, especially for the nearby MUIS where our observations show that the warm water reaching the cavity comes from the upper pycnocline rather than the mCDW. Deepening of the upper pycnocline in the polynya could prevent relatively warm water from reaching the base of the MUIS. The models of *Khazendar et al.* [2013] and *Gwyther et al.* [2014] suggest that a mixture of mCDW and cold water formed in the polynya

drives basal melt of the TIS. In years when the polynya is more active this mixture is cooler and the TIS basal melt is substantially reduced. Since the pathways by which warm water reaches the TIS cavity are unknown, our observations cannot assess the validity of the modeling output. However, the bathymetry used in these models does not capture the complex network of channels present near the TIS front. Our results indicate that if these topographic features are not resolved it is not possible to properly simulate the ice-ocean interactions at the TIS, suggesting that the modeled sensitivity of TIS basal melt rate to polynya activity might not be realistic.

Variability of most of the processes just described is influenced by local processes (e.g., coastal winds and polynya activity), suggesting that small-scale regional variability can drive changes in basal melt of the ice shelves on the Sabrina Coast. However, variability of mCDW intrusions onto the shelf may be driven by large-scale climate variability. *Spence et al*. [2014] show that the projected poleward shift of the southern hemisphere westerly winds at the end of the 21st century under sustained anthropogenic CO_2 emissions would cause a shoaling of the pycnocline depth on the continental slope, producing a thicker and warmer layer of mCDW on the continental shelf of the Sabrina Coast. Both local and remote processes therefore might affect the future ocean heat flux to the TIS and MUIS. Further surveys on the Sabrina Coast as well as ocean models with realistic bathymetry will be required to quantify the interannual variability of ocean heat flux to the cavities and to assess the processes that drive temporal variability of pycnocline depth and cross-shelf exchange.

5. Conclusions

Oceanographic data collected in the austral summer of 2015 provide the most comprehensive hydrographic survey of the Sabrina Coast continental shelf to date. In most of the region covered by our survey, we find warm mCDW in the bottom layer below fresh Winter Water. Glacial meltwater is widespread on the southern shelf at depths shallower than 300–400 m. These features are atypical for East Antarctica but resemble those observed in the Amundsen and Bellingshausen seas, where rapid basal melt and thinning of ice shelves in recent decades have been linked to inflow of mCDW to the ice-shelf cavities.

Relatively warm water drives high rates of ice-shelf basal melt on the Sabrina Coast, but access to the cavities is restricted to narrow troughs; bathymetric obstacles in uncharted areas presumably prevent the warmest water found on the shelf from accessing the ice-shelf cavities. Topographic features therefore strongly influence the ocean heat flux to ice shelves on the Sabrina Coast. Variations in pycnocline depth and cross-shelf exchange driven by changes in local and remote forcing may alter the temperature of the water reaching the ice-shelf cavities. Models suggest that under continued high emissions of greenhouse gases, ocean-initiated collapse of the Totten Ice Shelf leads to rapid ice loss from the Aurora Subglacial Basin, contributing several meters of global sea level rise in coming centuries [*Golledge et al*., 2015; *DeConto and Pollard*, 2016]. Our observations show that there is a substantial reservoir of heat on the continental shelf near the Totten Glacier, but the processes that control ocean heat transport to the ice-shelf cavity are not known. It is therefore critical to improve our understanding of the mechanisms regulating oceanic variability on the Sabrina Coast in order to predict the future contribution of the East Antarctic Ice Sheet to sea-level rise.

Acknowledgments
We thank the scientists, technicians, officers, and crew that participated to the R/V *Aurora Australis* expedition. The work was supported by the Australian Antarctic Research Program, the Australian Research Council's Special Research Initiative for the Antarctic Gateway Partnership, the Australian Climate Change Science Program, the Australian Government's Cooperative Research Centres Program through the Antarctic Climate & Ecosystems Cooperative Research Centre (ACE CRC), the National Environmental Science Program Earth System and Climate Change Hub, and Australia's Integrated Marine Observing System. Alessandro Silvano is supported by the Australian Government through the Australian Postgraduate Awards (APA) and the International Postgraduate Research Scholarships (IPRS) and by CSIRO and University of Tasmania through the Quantitative Marine Science PhD program. We thank Laurie Padman and one anonymous reviewer, as their comments greatly improved the manuscript. We want to thank Jason Roberts (Australian Antarctic Division, ACE CRC), Felicity Graham (University of Tasmania), and Will Hobbs (ACE CRC) for helpful discussions during the development of this work. Data are available from the Australian Antarctic Data Centre (https://data.aad.gov.au/).

References

Bindoff, N. L., M. A. Rosenberg, and M. J. Warner (2000), On the circulation and water masses over the Antarctic continental slope and rise between 80 and 150°E, *Deep Sea Res., Part II*, *47*(12–13), 2299–2326, doi:10.1016/S0967-0645(00)00038-2.

DeConto, R. M., and D. Pollard (2016), Contribution of Antarctica to past and future sea-level rise, *Nature*, *531*(7596), 591–597, doi:10.1038/nature17145.

Dee, D. P., et al. (2011), The ERA-Interim reanalysis: Configuration and performance of the data assimilation system, *Q. J. R. Meteorol. Soc.*, *137*, 553–597, doi:10.1002/qj.828.

Depoorter, M. A., J. L. Bamber, J. A. Griggs, J. T. M. Lenaerts, S. R. M. Ligtenberg, M. R. van den Broeke, and G. Moholdt (2013), Calving fluxes and basal melt rates of Antarctic ice shelves, *Nature*, *502*(7469), 89–92, doi:10.1038/nature12567.

Dupont, T. K., and R. B. Alley (2005), Assessment of the importance of ice-shelf buttressing to ice-sheet flows, *Geophys. Res. Lett.*, *32*, L04503, doi:10.1029/2004GL022024.

Dutrieux, P., J. De Rydt, A. Jenkins, P. R. Holland, H. K. Ha, S. H. Lee, E. J. Steig, Q. Ding, E. P. Abrahamsen, and M. Schroder (2014), Strong sensitivity of Pine Island ice-shelf melting to climatic variability, *Science*, *343*(6167), 174–178, doi:10.1126/science.1244341.

Foldvik, A., and T. Kvinge (1974), Conditional instability of sea-water at freezing-point, *Deep Sea Res. Oceanogr. Abstr.*, *21*(3), 169–174.

Fretwell, P., et al. (2013), Bedmap2: Improved ice bed, surface and thickness datasets for Antarctica, *Cryosphere*, *7*, 375–393, doi:10.5194/tc-7-375-2013.

Fyke, J. G., L. Carter, A. Mackintosh, A. J. Weaver, and K. J. Meissner (2010), Surface melting over ice shelves and ice sheets as assessed from modeled surface air temperatures, *J. Clim.*, *23*(7), 1929–1936, doi:10.1175/2009JCLI3122.1.
Gade, H. G. (1979), Melting of ice in sea water: A primitive model with application to the Antarctic ice shelf and icebergs, *J. Phys. Oceanogr.*, *9*, 189–198.
Gill, A. E. (1973), Circulation and bottom water production in the Weddell Sea, *Deep Sea Res. Oceanogr. Abstr.*, *20*(2), 111–140.
Golledge, N. R., D. E. Kowalewski, T. R. Naish, R. H. Levy, C. J. Fogwill, and E. G. W. Gasson (2015), The multi-millennial Antarctic commitment to future sea-level rise, *Nature*, *526*(7573), 421–425, doi:10.1038/nature15706.
Greenbaum, J. S., et al. (2015), Ocean access to a cavity beneath Totten Glacier in East Antarctica, *Nat. Geosci.*, *8*(4), 294–298, doi:10.1038/ngeo2388.
Gwyther, D. E., B. K. Galton-Fenzi, J. R. Hunter, and J. L. Roberts (2014), Simulated melt rates for the Totten and Dalton ice shelves, *Ocean Sci.*, *10*, 267–279, doi:10.5194/os10-267-2014.
Harig, C., and F. J. Simons (2015), Accelerated West Antarctic ice mass loss continues to outpace East Antarctic gains, *Earth Planet. Sci. Lett.*, *415*, 134–141, doi:10.1016/j.epsl.2015.01.029.
Hellmer, H. H., S. S. Jacobs, and A. Jenkins (1998), Oceanic erosion of a floating Antarctic glacier in the Amundsen Sea, in *Ocean, Ice, and Atmosphere: Interactions at the Antarctic Continental Margin, Antarct. Res. Ser.*, vol. 75, edited by S. S. Jacobs and R. F. Weiss, pp. 83–99, AGU, Washington, D. C.
Herraiz-Borreguero, L., I. Allison, M. Craven, K. W. Nicholls, and M. A. Rosenberg (2013), Ice shelf/ocean interactions under the Amery Ice Shelf: Seasonal variability and its effect on marine ice formation, *J. Geophys. Res. Oceans*, *118*, 7117–7131, doi:10.1002/2013JC009158.
Jacobs, S. S., A. F. Amos, and P. M. Bruchhausen (1970), Ross Sea oceanography and Antarctic bottom water formation, *Deep Sea Res. Oceanogr. Abstr.*, *17*(6), 935–962.
Jacobs, S. S., H. H. Hellmer, C. S. M. Doake, A. Jenkins, and R. M. Frolich (1992), Melting of ice shelves and the mass balance of Antarctica, *J. Glaciol.*, *38*(130), 375–387.
Jacobs, S. S., A. Jenkins, C. F. Giulivi, and P. Dutrieux (2011), Stronger ocean circulation and increased melting under Pine Island Glacier ice shelf, *Nat. Geosci.*, *4*(8), 519–523, doi:10.1038/ngeo1188.
Jacobs, S., C. Giulivi, P. Dutrieux, E. Rignot, F. Nitsche, and J. Mouginot (2013), Getz Ice Shelf melting response to changes in ocean forcing, *J. Geophys. Res. Oceans*, *118*, 4152–4168, doi:10.1002/jgrc.20298.
Jenkins, A. (1999), The impact of melting ice on ocean waters, *J. Phys. Oceanogr.*, *29*, 2370–2381.
Jenkins, A., and S. S. Jacobs (2008), Circulation and melting beneath George VI ice shelf, Antarctica, *J. Geophys. Res.*, *113*, C04013, doi:10.1029/2007JC004449.
Johnson, G. C. (2008), Quantifying Antarctic Bottom Water and North Atlantic Deep Water volumes, *J. Geophys. Res.*, *113*, C05027, doi:10.1029/2007JC004477.
Khazendar, A., M. P. Schodlok, I. Fenty, S. R. M. Ligtenberg, E. Rignot, and M. R. van den Broeke (2013), Observed thinning of Totten Glacier is linked to coastal polynya variability, *Nat. Commun.*, *4*, 2857, doi:10.1038/ncomms3857.
Kim, I., D. Hahm, T. S. Rhee, T. W. Kim, C.-S. Kim, and S. H. Lee (2016), The distribution of glacial meltwater in the Amundsen Sea, Antarctica, revealed by dissolved helium and neon, *J. Geophys. Res. Oceans*, *121*, 1654–1666, doi:10.1002/2015JC011211.
Kitade, Y., K. Shimada, T. Tamura, G. D. Williams, S. Aoki, Y. Fukamachi, F. Roquet, M. Hindell, S. Ushio, and K. I. Ohshima (2014), Antarctic Bottom Water production from the Vincennes Bay Polynya, East Antarctica, *Geophys. Res. Lett.*, *41*, 3528–3534, doi:10.1002/2014GL059971.
Li, X., E. Rignot, M. Morlighem, J. Mouginot, and B. Scheuchl (2015), Grounding line retreat of Totten Glacier, East Antarctica, 1996 to 2013, *Geophys. Res. Lett.*, *42*, 8049–8056, doi:10.1002/2015GL065701.
Li, X., E. Rignot, J. Mouginot, and B. Scheuchl (2016), Ice flow dynamics and mass loss of Totten Glacier, East Antarctica from 1989 to 2015, *Geophys. Res. Lett.*, *43*, 6366–6373, doi:10.1002/2016GL069173.
Liu, Y., J. C. Moore, X. Cheng, R. M. Gladstone, J. N. Bassis, H. Liu, J. Wen, and F. Hui (2015), Ocean-driven thinning enhances iceberg calving and retreat of Antarctic ice shelves, *Proc. Natl. Acad. Sci. U.S.A.*, *112*(11), 3263–3268, doi:10.1073/pnas.1415137112.
Marshall, J., and K. Speer (2012), Closure of the meridional overturning circulation through Southern Ocean upwelling, *Nat. Geosci.*, *5*(3), 171–180, doi:10.1038/ngeo1391.
Martinerie, P., D. Raynaud, D. M. Etheridge, J.-M. Barnola, and D. Mazaudier (1992), Physical and climatic parameters which influence the air content in polar ice, *Earth Planet. Sci. Lett.*, *112*(1–4), 1–13, doi:10.1016/0012-821X(92)90002-D.
Ohshima, K. I., et al. (2013), Antarctic Bottom Water production by intense sea-ice formation in the Cape Darnley Polynya, *Nat. Geosci.*, *6*(3), 235–240, doi:10.1038/ngeo1738.
Orsi, A. H., and C. L. Wiederwohl (2009), A recount of Ross Sea waters, *Deep Sea Res., Part II*, *56*(13–14), 778–795, doi:10.1016/j.dsr2.2008.10.033.
Padman, L., et al. (2012), Oceanic controls on the mass balance of Wilkins Ice Shelf, Antarctica, *J. Geophys. Res.*, *117*, C01010, doi:10.1029/2011JC007301.
Paolo, F. S., H. A. Fricker, and L. Padman (2015), Volume loss from Antarctic ice shelves is accelerating, *Science*, *348*(6232), 327–331, doi:10.1126/science.aaa0940.
Petty, A. A., D. L. Feltham, and P. R. Holland (2013), Impact of atmospheric forcing on Antarctic continental shelf water masses, *J. Phys. Oceanogr.*, *43*(5), 920–940, doi:10.1175/JPO-D-12-0172.1.
Picard, G., and M. Fily (2006), Surface melting observations in Antarctica by microwave radiometers: Correcting 26-year time series from changes in acquisition hours, *Remote Sens. Environ.*, *104*(3), 325–336, doi:10.1016/j.rse.2006.05.010.
Pritchard, H. D., S. R. M. Ligtenberg, H. A. Fricker, D. G. Vaughan, M. R. van den Broeke, and L. Padman (2012), Antarctic ice-sheet loss driven by basal melting of ice shelves, *Nature*, *484*(7395), 502–505, doi:10.1038/nature10968.
Randall-Goodwin, E., et al. (2015), Freshwater distributions and water mass structure in the Amundsen Sea Polynya region, Antarctica, *Elem. Sci. Anthropocene*, *3*(1), 000065, doi:10.12952/journal.elementa.000065.
Rignot, E., J. L. Bamber, M. R. van den Broeke, C. Davis, Y. Li, W. J. van de Berg, and E. van Meijgaard (2008), Recent Antarctic ice mass loss from radar interferometry and regional climate modelling, *Nat. Geosci.*, *1*, 106–110, doi:10.1038/ngeo102.
Rignot, E., S. Jacobs, J. Mouginot, and B. Scheuchl (2013), Ice-shelf melting around Antarctica, *Science*, *341*(6143), 266–270, doi:10.1126/science.1235798.
Rintoul, S. R. (1998), On the origin and influence of Adélie Land Bottom Water, in *Ocean, Ice, Atmosphere: Interactions at the Antarctic Continental Margin, Antarct. Res. Ser.*, vol. 75, edited by S. S. Jacobs and R. F. Weiss, pp. 151–171, AGU, Washington, D. C.
Rintoul, S. R., A. Silvano, B. Pena-Molino, E. van Wijk, M. A. Rosenberg, J. S. Greenbaum, and D. D. Blankenship (2016), Ocean heat drives rapid basal melt of Totten Ice Shelf, *Sci. Adv.*, *2*, e1601610, doi:10.1126/sciadv.1601610.
Rosenberg, M., and S. R. Rintoul (2016), Aurora Australis marine science cruise AU1402, Totten and Mertz CTDs and moorings—Oceanographic field measurements and analysis, unpublished report, 69 pp., ACE Coop. Res. Cent., Hobart, Australia.

Scambos, T., J. Bohlander, and B. Raup (1996), *Images of Antarctic Ice Shelves [2002-present]*, Natl. Snow and Ice Data Cent., Boulder, Colo., doi:10.7265/N5NC5Z4N.

Shadwick, E. H., S. R. Rintoul, B. Tilbrook, G. D. Williams, N. Young, A. D. Fraser, H. Marchant, J. Smith, and T. Tamura (2013), Glacier tongue calving reduced dense water formation and enhanced carbon uptake, *Geophys. Res. Lett.*, *40*, 904–909, doi:10.1002/grl.50178.

Shepherd, A., D. Wingham, and E. Rignot (2004), Warm ocean is eroding West Antarctic Ice Sheet, *Geophys. Res. Lett.*, *31*, L23402, doi: 10.1029/2004GL021106.

Silvano, A., S. R. Rintoul, and L. Herraiz-Borreguero (2016), Ocean-ice shelf interaction in East Antarctica, *Oceanography*, *29*(4), 130–143, doi: 10.5670/oceanog.2016.105.

Smith, W. H. F., and D. T. Sandwell (1997), Global seafloor topography from satellite altimetry and ship depth soundings, *Science*, *277*, 1956–1962.

Spence, P., S. M. Griffies, M. H. England, A. M. C. Hogg, O. A. Saenko, and N. C. Jourdain (2014), Rapid subsurface warming and circulation changes of Antarctic coastal waters by poleward shifting winds, *Geophys. Res. Lett.*, *41*, 4601–4610, doi:10.1002/2014GL060613.

St-Laurent, P., J. M. Klinck, and M. S. Dinniman (2015), Impact of local winter cooling on the melt of Pine Island Glacier, Antarctica, *J. Geophys. Res. Oceans*, *120*, 6718–6732, doi:10.1002/2015JC010709.

Sun, S., S. L. Cornford, D. E. Gwyther, R. M. Gladstone, B. K. Galton-Fenzi, L. Zhao, and J. C. Moore (2016), Impact of ocean forcing on the Aurora Basin in the 21st and 22nd centuries, *Ann. Glaciol.*, *57*, 79–86, doi:10.1017/aog.2016.27.

Tamura, T., K. I. Ohshima, A. D. Fraser, and G. D. Williams (2016), Sea ice production variability in Antarctic coastal polynyas, *J. Geophys. Res. Oceans*, *121*, 2967–2979, doi:10.1002/2015JC011537.

Thoma, M., A. Jenkins, D. Holland, and S. Jacobs (2008), Modelling Circumpolar Deep Water intrusions on the Amundsen Sea continental shelf, Antarctica, *Geophys. Res. Lett.*, *35*, L18602, doi:10.1029/2008GL034939.

Wåhlin, A. K., X. Yuan, G. Bjork, and C. Nohr (2010), Inflow of warm circumpolar deep water in the central Amundsen Shelf, *J. Phys. Oceanogr.*, *40*(6), 1427–1434, doi:10.1175/2010JPO4431.1.

Williams, G. D., A. J. S. Meijers, A. Poole, P. Mathiot, T. Tamura, and A. Klocker (2011), Late winter oceanography off the Sabrina and BANZARE coast (117–128 E), East Antarctica, *Deep Sea Res., Part II*, *58*(9–10), 1194–1210, doi:10.1016/j.dsr2.2010.10.035.

Williams, G. D., et al. (2016), The suppression of Antarctic bottom water formation by melting ice shelves in Prydz Bay, *Nat. Commun.*, *7*, 12,577, doi:10.1038/ncomms12577.

Wouters, B., A. Martin-Español, V. Helm, T. Flament, J. M. van Wessem, S. R. M. Ligtenberg, M. R. van den Broeke, and J. L. Bamber (2015), Dynamic thinning of glaciers on the Southern Antarctic Peninsula, *Science*, *348*(6237), 899–903, doi:10.1126/science.aaa5727.

Zhang, X., A. F. Thompson, M. M. Flexas, F. Roquet, and H. Bornemann (2016), Circulation and meltwater distribution in the Bellingshausen Sea: From shelf break to coast, *Geophys. Res. Lett.*, *43*, 6402–6409, doi:10.1002/2016GL068998.